

Phase relations in the system MgO-FeO-SiO₂ to 50 GPa and 2000°C: An application of experimental techniques using multianvil apparatus with sintered diamond anvils

Yoshinori Tange,^{1,2} Eiichi Takahashi,¹ Yu Nishihara,^{1,2} Ken-ichi Funakoshi,³ and Nagayoshi Sata⁴

Received 23 June 2008; revised 31 October 2008; accepted 2 December 2008; published 28 February 2009.

[1] Phase relations in the system MgO-FeO-SiO₂ were investigated between 22 and 47 GPa at 1500°C and 2000°C using multianvil apparatus with sintered diamond anvils. Synthesized samples were analyzed with electron microprobe, analytic transmission electron microscopy, and X-ray diffraction using synchrotron radiation. Univariant compositions of (Mg,Fe)SiO₃ perovskite and (Mg,Fe)O magnesiowüstite coexisting with SiO₂ stishovite were determined as functions of pressure and temperature. The maximum iron solubility in perovskite corresponding to the univariant composition gradually increases with increasing pressure and temperature to be more than 30 mol % at 2000°C and pressures above 40 GPa, and a significant pressure effect was found in Fe-Mg partitioning between perovskite and magnesiowüstite in pressures between 22 and 35 GPa. The iron content of magnesiowüstite dramatically increases from 50 to greater than 90 mol % with increasing pressure, and the Fe-Mg distribution coefficients between perovskite and magnesiowüstite, $K_D = (X_{\text{Fe}}^{\text{Pv}}/X_{\text{Mg}}^{\text{Pv}})/(X_{\text{Fe}}^{\text{Mw}}/X_{\text{Mg}}^{\text{Mw}})$, decrease to less than 0.05. This significant pressure effect in Fe-Mg partitioning causes strong concentration of ferrous iron in magnesiowüstite with increasing depth in the lower mantle.

Citation: Tange, Y., E. Takahashi, Y. Nishihara, K. Funakoshi, and N. Sata (2009), Phase relations in the system MgO-FeO-SiO₂ to 50 GPa and 2000°C: An application of experimental techniques using multianvil apparatus with sintered diamond anvils, *J. Geophys. Res.*, 114, B02214, doi:10.1029/2008JB005891.

1. Introduction

[2] The Earth's lower mantle contains more than half the mass of the planet, and the system MgO-FeO-SiO₂ is fundamental to our understanding of its constituents and dynamics because the total amounts of MgO, FeO, and SiO₂ make up more than 90 wt % of the bulk silicate Earth [e.g., Ringwood, 1975]. As a result of this, the phase relations in the system MgO-FeO-SiO₂ have been extensively investigated using high-pressure and high-temperature techniques [e.g., Yagi *et al.*, 1979a; Ito and Yamada, 1982; Ito *et al.*, 1984; Ito and Takahashi, 1989; Mao *et al.*, 1997]. These studies have revealed that (Mg,Fe)SiO₃ perovskite (Pv) and (Mg,Fe)O magnesiowüstite (Mw) are dominant mineral phases in the Earth's lower mantle [e.g., Ito *et al.*, 1984; Ito and Takahashi, 1989].

[3] High-pressure and high-temperature phase equilibria in the MgO-FeO-SiO₂ system have been studied using the

laser-heated diamond anvil cell (LHDAC) and the Kawai-type multianvil apparatus (KMA) [Kawai and Endo, 1970]. Using LHDAC at 20 GPa and ~1000°C, Yagi *et al.* [1979a] provided the first report on the maximum solubility of iron in Pv as 0.20 in X_{Fe} and the chemical composition of coexisting Mw. In an early KMA study at 26 GPa, Ito *et al.* [1984] found that Fe-Mg distribution coefficients between Pv and Mw are sensitive to the bulk Mg/Fe ratio. In their work, the maximum iron solubility in Pv was reported as 0.11 in X_{Fe} at 1600°C, which was lower than that reported by Yagi *et al.* [1979a]. In KMA investigations at 26 GPa, Fei *et al.* [1996] determined the maximum iron solubility in Pv as 0.07–0.12 in X_{Fe} at 1150–1750°C, and Katsura and Ito [1996] determined Fe-Mg partitioning between Pv and Mw, respectively. Mao *et al.* [1997] then performed extensive experiments up to 55 GPa using LHDAC with synchrotron-based X-ray diffraction (XRD) measurements, and found multivariable dependences in Fe-Mg partitioning under lower mantle conditions as a function of pressure, temperature, and bulk Mg/Fe ratio. However, later studies using LHDAC reported significantly different pressure effects for Fe-Mg partitioning [Andrault, 2001; Kobayashi *et al.*, 2005]. In addition, there are some inconsistencies in the phase relations and Fe-Mg partitioning between the results based on KMA below 30 GPa and those based on LHDAC at higher pressures. Thus, phase equilib-

¹Department of Earth and Planetary Sciences, Tokyo Institute of Technology, Meguro, Tokyo, Japan.

²Now at Geodynamics Research Center, Ehime University, Matsuyama, Ehime, Japan.

³Japan Synchrotron Radiation Research Institute, Sayo, Hyogo, Japan.

⁴Institute for Research on Earth Evolution, Japan Agency for Marine-Earth Science and Technology, Yokosuka, Kanagawa, Japan.

ria in the system MgO-FeO-SiO₂ are still uncertain over the bulk of lower mantle conditions.

[4] Although KMA has the advantage of generating stable high *P-T* conditions, the experimental pressure is limited below 30 GPa when the usual tungsten carbide anvils are used. For this reason, static experiments at deep lower mantle conditions have been performed only by LHDAC. Recent technical developments in experiments with sintered diamond (SD) anvils allow us to achieve the Earth's mid lower mantle conditions using KMA [e.g., Ito *et al.*, 2005; Tange *et al.*, 2008]. Using this new technique we performed a series of high *P-T* experiments under deep lower mantle conditions in the system MgO-FeO-SiO₂ to clarify *P-T* effects on the phase relations.

2. Experimental Procedures

[5] The starting material was a (Mg_{0.5}Fe_{0.5})SiO₃ clinopyroxene, which was synthesized from reagents (MgO, Fe₂O₃ and SiO₂) by heating at 1 atm and 1250°C for 50 h under a controlled oxygen fugacity (QFM – 2 log units). The chemical composition and phases present were examined by an electron-probe microanalyzer (EPMA; JXA-8800M, JEOL Ltd.) and a microfocus X-ray diffractometer (MXRD; RINT-2000, Rigaku Co.). The synthesized sample consists of clinopyroxene with a homogeneous composition of (Mg_{0.53}Fe_{0.47})SiO₃ and minor amounts of olivine [(Mg_{0.44}Fe_{0.56})₂SiO₄] and cristobalite (SiO₂). The amounts of olivine and cristobalite were evaluated, from backscattered electron images (BEI), to be less than 3 vol %.

[6] High-pressure and high-temperature experiments were performed using a KMA, known as SPEED-Mk.II [Katsura *et al.*, 2004], installed at BL04B1 beam line in SPring-8. In situ X-ray diffraction (XRD) measurements with the synchrotron radiation were carried out using white X-rays and the energy-dispersive method with a Ge solid-state detector and a horizontal goniometer [Utsumi *et al.*, 1998]. In the in situ high *P-T* experiments, Au was employed as an internal pressure standard and the equation of state of Tsuchiya [2003] was used as the pressure scale. Experiments below 30 GPa were carried out with another apparatus installed at Tokyo Institute of Technology (Sakura-2500), and pressures were determined from a relationship between the applied press load and the generated pressure. The relationship was calibrated in advance using the ilmenite-Pv phase transition in MgSiO₃ [Ono *et al.*, 2001]. Eight SD cubes of 14.0 mm with truncated edge lengths of 2.0 mm were used as the second stage anvils (SUMIDIA WD-700; Sumitomo Electric Industries, Co., Ltd). The SD has a Co binder and is therefore electrically conductive. A pressure medium made of semisintered MgO doped with 5 wt % Cr₂O₃ (OM-CR; Mino Ceramic Co., Ltd.) and composite gaskets of baked and raw pyrophyllite were used (Figure 1a). Figure 1b shows a cross section of the high-pressure cell assembly. A LaCrO₃ cylindrical furnace was used, with graphite windows along the X-ray path in order to obtain clear XRD profiles. The sample and the pressure marker were packed in capsules made of graphite. Au powder was mixed with the starting material as the pressure standard in experiments at 1500°C, and a powder mixture of Au and MgO was used as the pressure standard in experiments at 2000°C. Temperatures were

measured by W₉₇Re₃-W₇₅Re₂₅ thermocouples (TC), and the hot junction of the TC was in the center of the cylindrical furnace. At first, pressure was increased at room temperature, and then temperature was increased to the target value (1500 or 2000°C) and held for at least 30 min. Samples were then quenched and recovered at ambient conditions. Details of similar experimental techniques are described by Tange *et al.* [2008].

[7] Phases present in the samples were determined with MXRD, and chemical compositions of those phases were measured using EPMA or an analytical transmission electron microscope (ATEM; JEM-2010, JEOL Ltd). All of the recovered run products were mounted in epoxy and coated with carbon, and analyzed with an EPMA at Tokyo Institute of Technology. Wavelength-dispersive spectrometers (WDS) were employed using a 15 kV accelerating voltage and 1.2×10^{-8} A beam current [e.g., Tuff *et al.*, 2005]. In run products in which grain growth was not sufficient, we reduced the beam current to 1.2×10^{-9} A in order to obtain a higher-spatial resolution in the chemical analyses. ATEM analyses were carried out in cases where chemical compositions of coexisting phases were not determined because of beam-overlapping effects in the EPMA analyses. For the ATEM analyses, we prepared specimens using an Ar ion-beam spatter after mechanically polishing both sides to ~ 0.01 mm in thickness. The chemical analyses were carried out using a TEM operated at 200 kV, combining Oxford Inca energy-dispersive spectrometry system with an ultra-thin window. All of the chemical analyses were made only for very thin parts of samples where electron transmission rates were more than 95%, and thin film approximation can be made [Takafuji *et al.*, 2004; Murakami *et al.*, 2005]. After the EPMA and ATEM analysis, we carried out XRD measurements at ambient conditions using synchrotron radiation; this is because MXRD does not have enough *d* value resolution to determine lattice parameters precisely. Angle-dispersive powder XRD measurements were performed with an imaging plate (IP; R-AXIS, Rigaku Co.) installed at BL10XU beam line, SPring-8 [Watanuki *et al.*, 2001]. The incident monochromatic X-ray was collimated to 0.1 mm in diameter, and the transmission XRD measurements were carried out through samples prepared as specimens with ~ 0.1 mm in thickness. The film distance from samples to the IP, wavelength of the monochromatic X-ray, tilt angles of the IP, and pixel sizes of the IP reader were calibrated from lattice parameters of a CeO₂ standard. The wavelength of the monochromatic X ray was 0.41693(8) Å (where values in parentheses indicate standard deviation).

3. Results and Discussion

3.1. Chemical Analyses

[8] A total of nine experiments were performed between 22 and 47 GPa at temperatures of 1500°C or 2000°C (Table 1). Temperatures were successfully measured by the TC except for one run (M135). In the experiment in which the TC did not work, the temperature was estimated from a relationship between generated temperatures and supplied electrical powers in the same run. Temperature fluctuations during heating were less than 5°C, even at 2000°C. There was no significant pressure change (less than 1 GPa) over the heating duration. In every experimental product, the graphite

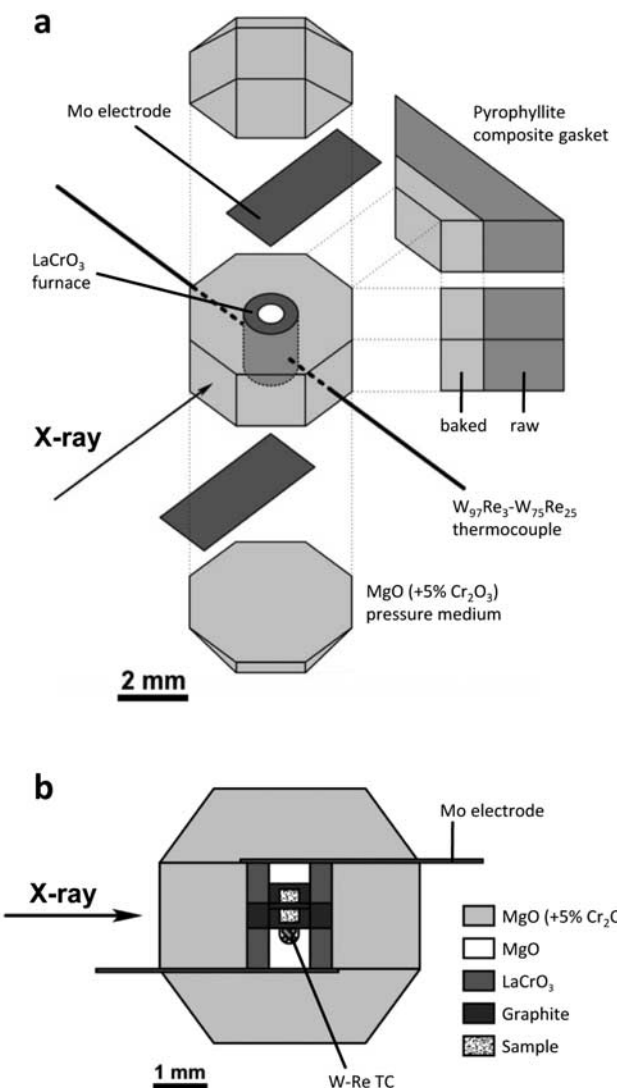


Figure 1. Schematic illustrations of (a) the cell assembly used in the high *P-T* experiments and (b) a cross section of the cell assembly used in the experiments at 2000°C. A single-capsule assembly was used in the experiments at 1500°C.

capsules transformed to diamond. MXRD confirmed that the three phases of Pv, Mw, and stishovite (St) coexisted in all of the run products. Since each sample is in a three-component

system, the coexistence of three phases (Pv + Mw + St) at a given pressure and temperature indicates that Pv and Mw have univariant compositions assuming chemical equilibrium. This univariant composition of Pv is also the maximum iron content of this phase at a given *P-T* condition.

[9] All recovered samples were analyzed with EPMA, and BEIs of typical run products are shown in Figure 2. White spots in Figures 2a and 2b are the Au powder pressure marker mixed with the starting material. The coexistence of Pv, Mw, and St was also confirmed by EPMA analyses. Variations in the grain sizes of the phases were observed in the experiments at different pressures at 1500°C (Figures 2a and 2b). In contrast, there was no significant influence of pressure at 2000°C (Figures 2c and 2d). The phase relations and volume fractions of the phases were estimated from the BEI. Phase combinations in matrix areas change from Mw + St to Pv + Mw between Figure 2a and 2b, and the result implies that the nearest tie line to the bulk composition changes from Mw-St to Pv-Mw in the MgO-FeO-SiO₂ ternary system. The volume fractions correspond to distances between the bulk composition and each composition of phases present. For example, when the composition of Pv is close to the bulk composition, the volume fraction of Pv increases and those of Mw and St decrease (Figures 2c and 2d). These observations indicate that the Pv-Mw tie line moved toward the starting composition with increasing pressure.

[10] Results of the chemical analyses are summarized in Table 2. The chemical compositions of Pv and Mw synthesized at 2000°C were easily determined by EPMA because grains were large enough to perform accurate chemical analysis without beam overlap with neighboring grains. In the run products synthesized at 1500°C, the grain size was not large enough to determine the chemical composition, and the compositions of Pv and Mw were therefore determined from the compositional tie lines between Pv and Mw, or Mw and St that result from beam overlap with neighboring grains. For the run products synthesized at 1500°C above 35 GPa (M134 and M135), ATEM analyses were carried out because the grain size was especially small and the tie line could not be identified. In the ATEM analyses, Mw was easily distinguished and its chemical composition could be determined accurately, and the compositions of Pv were determined using the tie lines between Pv and St. On the basis of the analyses described above, chemical compositions of Pv and Mw were determined with small uncertainties (less than 0.02 in molar fraction). In order to

Table 1. Experimental Conditions and Present Phases^a

Run	Load (MN)	Volume of Au (Å ³)	Pressure (GPa)	Temperature (°C)	Duration (min)	Sample	Present Phase
U88 ^b	2.95	—	25	1500	30	MgSiO ₃ glass	Pv, St
U93 ^b	2.95	—	25	1500	30	En ₅₀ + Au	Pv, Mw, St
M136	3.30	62.31(9)	28.6(5)	1500	40	En ₅₀ + Au	Pv, Mw, St
M134	5.00	60.35(7)	37.6(4)	1500	40	En ₅₀ + Au	Pv, Mw, St
M135	8.10	58.76(9)	46.5(6)	1500 ^c	40	En ₅₀ + Au	Pv, Mw, St
U99 ^b	2.95	—	22	2000	30	En ₅₀ , MgO + Au	Pv, Mw, St
M204	3.30	63.61(16)	27.1(8)	2000	30	En ₅₀ , MgO + Au	Pv, Mw, St
M224	5.00	61.82(7)	34.1(4)	2000	30	En ₅₀ , MgO + Au	Pv, Mw, St
M183	8.10	59.95(8)	43.1(5)	2000	30	En ₅₀ , MgO + Au	Pv, Mw, St

^aValues in parentheses indicate standard deviation.

^bHigh *P-T* experiments were carried out without in situ X-ray observations.

^cTemperature was estimated from the relationship between temperatures and supplied electrical power up to 1200°C.

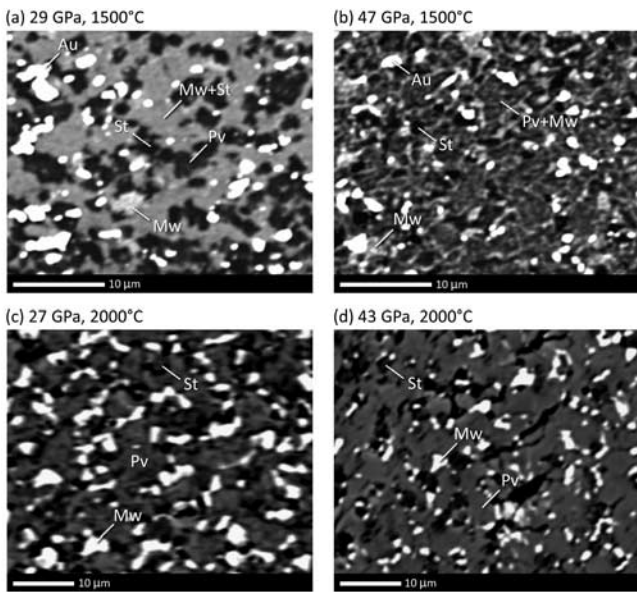


Figure 2. An example of the backscattered electron images of run products. Au powder was mixed into the starting material as a pressure standard in Figures 2a and 2b.

compare the results of the ATEM analyses to those of EPMA analyses, another ATEM analysis was carried out for M183, in which the chemical compositions of Pv and Mw were precisely determined by EPMA. The chemical compositions were determined with ATEM as $X_{\text{Fe}}^{\text{Pv}} = 0.30(2)$ and $X_{\text{Fe}}^{\text{Mw}} = 0.92(2)$, and the results were consistent with the EPMA results [$X_{\text{Fe}}^{\text{Pv}} = 0.318(13)$, $X_{\text{Fe}}^{\text{Mw}} = 0.904(2)$]. The results of the chemical analyses show that the univariant triangle shifts to the iron-rich side with increasing pressure, and the Pv-Mw tie line shifts toward the starting composition of $(\text{Mg}_{0.5}\text{Fe}_{0.5})\text{SiO}_3$. This result is consistent with the BEI observations.

3.2. X-V Relationship in (Mg,Fe)SiO₃ Perovskite

[11] In order to determine a relationship between lattice volumes and iron contents in Pv, XRD measurements were performed using synchrotron radiation under ambient conditions. The products of runs U88, M134, M135, M136 and M183, for which the FeSiO₃ contents in (Mg,Fe)SiO₃ Pv are from 0.00 to 0.32 (Table 2), were measured. Lattice parameters and volumes were calculated using diffraction peaks integrated from full circles of the Debye rings. An example of the integrated one-dimensional XRD profiles is shown in Figure 3. In the XRD profile of runs M134, M135, M136, and M183, all observed peaks were indexed by the diffractions from Pv, Mw, St, and Au (except M183) without any unidentified peak.

[12] The lattice volume of MgSiO₃ Pv has been measured by a number of authors, and the reported values of the lattice volume range from 162.0 to 162.75 Å³ [Liu, 1974; Ito and Matsui, 1978; Yagi et al., 1978; Mao et al., 1991; Wang et al., 1994; Funamori et al., 1996; Fiquet et al., 1998]. In this study, the lattice parameters of MgSiO₃ Pv were determined precisely using 33 diffraction peaks and the lattice volume was found to be 162.373(16) Å³, which is close to the average of previous studies and strongly consistent with the value reported by Ito and Matsui

[1978] [162.35(2) Å³]. The lattice parameters of iron-bearing (Mg,Fe)SiO₃ Pv were determined with 19–28 diffraction peaks, and the obtained values are summarized in Table 3. Relationships between lattice parameters and iron contents in Pv are shown in Figure 4. The variations of lattice parameters as a function of iron content are linear, within the uncertainties of the chemical analyses, and the X - V relationship is described by $V(\text{Å}^3) = 162.373 + 5.94X_{\text{Fe}}^{\text{Pv}}$. Present results are consistent with previous studies [Yagi et al., 1979b; Ito and Yamada, 1982; Mao et al., 1991; Fei et al., 1996] and the X - V relation is very consistent with that observed by Ito and Yamada [1982]. (Mg,Fe)SiO₃ Pv has a fictive end-member of FeSiO₃, and the volume of FeSiO₃ Pv can be estimated from the X - V relation to be 168.31(10) Å³ which is consistent with that reported by Fei et al. [1996].

[13] St exists in all samples, and we found its lattice volume to be 46.55(3) Å³. The previously reported lattice volumes of St at ambient conditions scatter from 46.50 to 46.62 Å³ [Ito et al., 1974; Endo et al., 1986; Ross et al., 1990; Liu et al., 1999; Andrault et al., 1998, 2003; Yamakawa et al., 2002; Nishihara et al., 2005]. The present result is close to the mean value of the previous studies. This consistency suggests that the chemical composition of St synthesized in the present experiments is close to pure SiO₂.

[14] The XRD profiles of Mw have strange characteristics compared to those of Pv and St. Although the Debye rings of Pv and St represented “perfectly round” circles in the original 2D-XRD profiles, coexisting Mw yielded the “distorted” Debye rings. The Debye rings of Pv and St were integrated as “straight” lines in another 2D form of $2\theta-\psi$ (azimuth angle) profile, in other words, the 2θ angles were constant for each diffraction plane. However, Mw yielded the broad and “winding” $\psi(2\theta)$ profiles with ~180° cycle in ψ angle. Therefore it was impossible to determine the d values precisely in Mw. These characteristics were significant in the samples synthesized at 1500°C. The small grain size less than 1 μm (Figures 2a and 2b) and an orientated lattice distortion are possible to explain the characteristics. However, in this study, information was not enough to discuss any more. A study focused on the currently observed characteristics in Mw should be conducted in future.

3.3. Pressure Dependence of the Phase Relations

[15] The phase relations in the MgO-FeO-SiO₂ system were determined in terms of univariant compositions of Pv and Mw under broad P - T conditions. In this system, the

Table 2. Results of the Chemical Analyses^a

Run	Pressure (GPa)	Temperature (°C)	$X_{\text{Fe}}^{\text{Pv}}$	$X_{\text{Fe}}^{\text{Mw}}$	K_D ^b
U93	25	1500	0.163(3)	0.485(5)	0.207(5)
M136	29	1500	0.162(7)	0.70(2)	0.083(6)
M134	38	1500	0.211(12) ^c	0.868(7) ^c	0.041(3)
M135	47	1500	0.248(16) ^c	0.921(4) ^c	0.028(2)
U99	22	2000	0.183(4)	0.6350(12)	0.129(4)
M204	27	2000	0.257(4)	0.795(5)	0.089(2)
M224	34	2000	0.290(10)	0.858(6)	0.068(4)
M183	43	2000	0.318(13)	0.904(2)	0.050(3)

^aValues in parentheses indicate standard deviation.

^b $K_D = (X_{\text{Fe}}^{\text{Pv}}/X_{\text{Mg}}^{\text{Pv}})/(X_{\text{Fe}}^{\text{Mw}}/X_{\text{Mg}}^{\text{Mw}})$.

^cDetermined by ATEM.

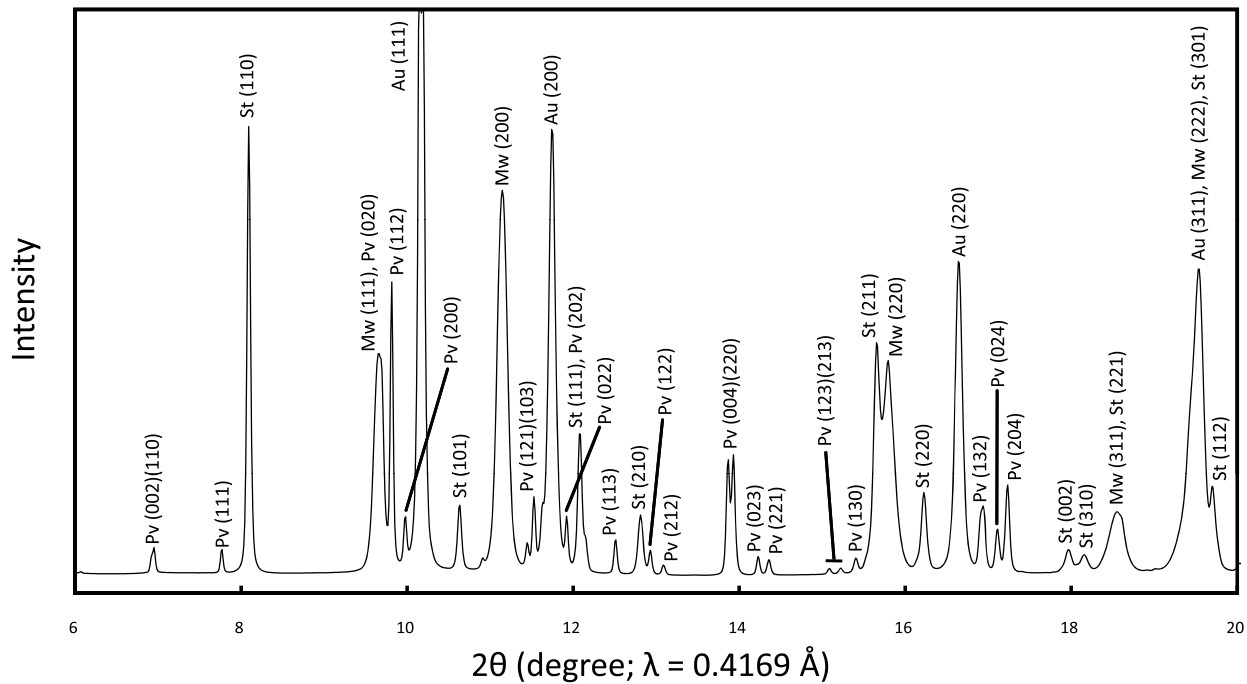


Figure 3. XRD profile of M136 at ambient conditions. $(\text{Mg}_{0.84}\text{Fe}_{0.16})\text{SiO}_3$ perovskite, $(\text{Mg}_{0.30}\text{Fe}_{0.70})\text{O}$ magnesiowüstite, St, and Au coexist in the run product.

maximum FeSiO₃ solubility in $(\text{Mg},\text{Fe})\text{SiO}_3$ Pv at a given $P-T$ is determined by the univariant composition of Pv. Figure 5a shows an example of the ternary phase diagrams in the MgO-FeO-SiO₂ system determined at 25 GPa and 1500°C and 43 GPa and 2000°C. The phase relation at 25 GPa and 1500°C was generally consistent with those found in previous studies performed by KMA at 26 GPa [Ito and Yamada, 1982; Ito et al., 1984] (Figure 5b). The phase relation at 20 GPa and ~1000°C reported by Yagi et al. [1979a] using LHDAC was consistent with our result at 22 GPa and 2000°C (Figure 5b and Table 2). In addition to the consistencies with the previous studies at pressures below 26 GPa, we found a significant pressure dependence and modest temperature dependence in the phase relations (Figure 5a). With increasing pressure, the univariant composition of Mw shifts to the increasingly iron-rich side and also the univariant triangle (Pv + Mw stability field) shifts to the iron-rich side. With increasing temperature, the univariant composition of Pv slightly shifts to the iron rich composition (Table 2).

[16] The pressure dependence of the phase relations can be shown as a pseudobinary phase diagram in $\text{MgSiO}_3\text{-FeSiO}_3$ system (Figure 6). The FeSiO₃-solubility limit in Pv gradually increases with increasing pressure, and expands to more than 30 mol % at 2000°C and pressures above 40 GPa. In addition to the pressure dependence of the univariant composition of Pv, we found a large pressure dependence in the univariant composition of Mw. The univariant composition of Mw dramatically increases with increasing pressure between 22 and 35 GPa, and the Pv + Mw + St stability field expands to the iron-rich side (Figure 6a). The expansion becomes less significant above 35 GPa. These results are generally consistent with the previous experiments

performed by KMA (at ~26 GPa) [Ito and Yamada, 1982; Ito et al., 1984] and LHDAC [Mao et al., 1997] (Figure 6b).

[17] Figure 6c shows the phase relations calculated on the basis of the thermodynamic parameters adopted by Akaogi et al. [1998]. Our experimental results and the thermodynamic calculation are qualitatively consistent in both pressure and temperature dependences in the univariant compositions of Mw. However, the thermodynamic calculation shows a narrow stability field of Pv even at 2000°C compared with our experimental results and those of Mao et al. [1997]. In addition, the calculated maximum iron solubility is inconsistent with the experimental results both in the pressure and temperature dependence. One possible reason for the discrepancy is an uncertainty in the thermodynamic and thermoelastic properties of FeSiO₃ Pv.

4. Fe-Mg Partitioning Between Perovskite and Magnesiowüstite

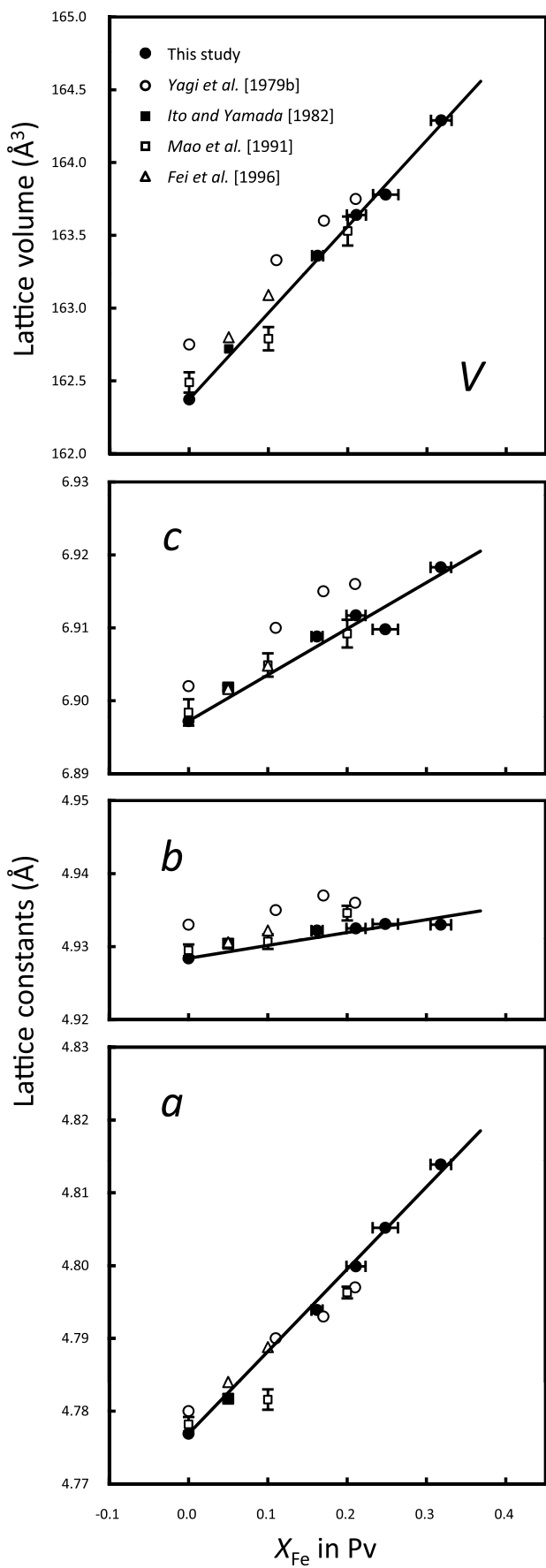
4.1. Thermodynamics in the Fe-Mg Substitution

[18] As a consequence of the pressure effect on the phase relations (Figure 6a), Fe-Mg distribution coefficients be-

Table 3. Lattice Parameters of $(\text{Mg},\text{Fe})\text{SiO}_3$ Perovskite^a

Run	X_{Fe}	a (Å)	b (Å)	c (Å)	V (Å ³)
U88	0.000	4.7769(3)	4.9284(3)	6.8972(4)	162.373(16)
M136	0.162(7)	4.7939(4)	4.9322(4)	6.9088(5)	163.36(2)
M134	0.211(12)	4.7999(6)	4.9325(5)	6.9117(8)	163.64(3)
M135	0.248(16)	4.8052(10)	4.9331(10)	6.9098(12)	163.78(5)
M183	0.318(13)	4.8139(6)	4.9330(7)	6.9183(8)	164.29(4)

^aValues in parentheses indicate standard deviation.



tween Pv and Mw, $K_D = (X_{\text{Fe}}^{\text{Pv}}/X_{\text{Mg}}^{\text{Pv}})/(X_{\text{Fe}}^{\text{Mw}}/X_{\text{Mg}}^{\text{Mw}})$, significantly decrease with increasing pressure. With increasing pressure (from 25 to 50 GPa), the K_D value decreases from 0.21 to less than 0.03 at 1500°C, and a similar pressure effect is observed at 2000°C (Table 2). Figure 7 shows the K_D values in the system MgO-FeO-SiO₂ as a function of $X_{\text{Fe}}^{\text{Mw}}$. The behavior of the K_D value at 23–25 GPa has been extensively investigated in previous studies using KMA [Katsura and Ito, 1996; Frost and Langenhorst, 2002]. Between 23 and 25 GPa, the compositional dependence of the K_D value is significant mainly due to the nonideal nature of magnesiowüstite solid solution, while the temperature dependence is small. Our data at 22 and 25 GPa are consistent with the trend of those previous studies. At pressures higher than 25 GPa, the K_D deviates from the trend to lower values with increasing $X_{\text{Fe}}^{\text{Mw}}$. The K_D values determined in this study represent the lowest limits at each P - T condition because those are derived from the Fe-saturated Pv and the coexisting univariant Mw.

[19] The ion exchange reaction for Fe-Mg partitioning between Pv and Mw is



For reaction (1), the distribution coefficient K_D can be expressed by

$$RT \ln K_D = -\Delta G^\circ(P, T) + W^{\text{Pv}}(1 - 2X_{\text{Fe}}^{\text{Pv}}) - W^{\text{Mw}}(1 - 2X_{\text{Fe}}^{\text{Mw}}), \quad (2)$$

where W^{Pv} and W^{Mw} are the nonideal parameters for Pv and Mw, respectively. The $\Delta G^\circ(P, T)$ is a variation in the Gibbs free energy for reaction (1). If changes in enthalpy, entropy, and volume for reaction (1) (ΔH° , ΔS° , and ΔV°) are assumed to be constant at corresponding P - T conditions, the $\Delta G^\circ(P, T)$ is simply expressed by

$$\Delta G^\circ(P, T) = \Delta H^\circ - T\Delta S^\circ + P\Delta V^\circ. \quad (3)$$

From equations (2) and (3), it can be clearly seen that the pressure dependence of the K_D at a constant chemical composition and constant temperature is directly related to the ΔV° value. Therefore, the negative pressure dependence of K_D observed in this study corresponds to a positive value of the volume change for reaction (1) ($\Delta V^\circ > 0$).

[20] The ΔV° value at ambient conditions can be calculated from the molar volume of MgSiO₃(Pv), FeSiO₃(Pv), MgO(Mw), and FeO(Mw). The molar volume for fictive end-member of FeSiO₃ Pv was estimated from the relationship between the composition and volume in (Mg,Fe)SiO₃ Pv solid solution determined in this study (Figure 4), and those of other end-members are precisely known on the basis of direct measurements. The ΔV° value at ambient conditions is calculated to be $\Delta V^\circ = -0.11 \pm 0.02 \text{ cm}^3/\text{mol}$ using the

Figure 4. Relationships between lattice parameters and iron contents in Pv ($X_{\text{Fe}}^{\text{Pv}}$) at ambient conditions along with previously measured results. The relationship between lattice volumes and $X_{\text{Fe}}^{\text{Pv}}$ is determined as $V (\text{\AA}^3) = 162.373 + 5.94X_{\text{Fe}}^{\text{Pv}}$ in this study.

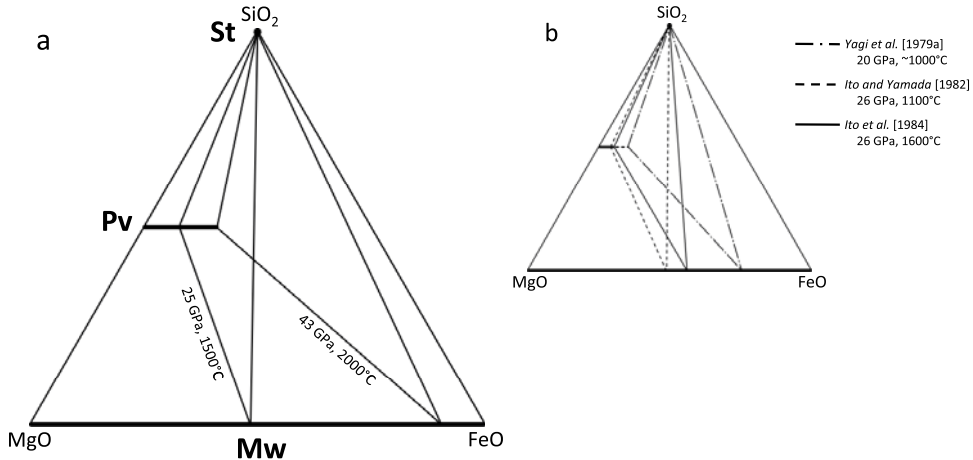


Figure 5. Ternary phase diagrams in the system MgO-FeO-SiO₂ determined (a) at 25 GPa and 1500°C, and 43 GPa and 2000°C (b) along with the previously reported phase relations below 26 GPa.

following values of molar volume for end-members: $V_{\text{MgSiO}_3} (\text{Pv}) = 24.445 \pm 0.002 \text{ cm}^3/\text{mol}$ and $V_{\text{FeSiO}_3} (\text{Pv}) = 25.339 \pm 0.015 \text{ cm}^3/\text{mol}$ (this study); $V_{\text{MgO}} (\text{Mw}) = 11.248 \text{ cm}^3/\text{mol}$ and $V_{\text{FeO}} (\text{Mw}) = 12.250 \text{ cm}^3/\text{mol}$ [Akaoji *et al.*, 1998]. This negative value of $\Delta V^\circ = -0.11 \pm 0.02 \text{ cm}^3/\text{mol}$ contrasts with the conclusion based on Fe-Mg partitioning ($\Delta V^\circ > 0$). One of the possible reasons for this inconsistency is that the simple assumption of constant ΔH° , ΔS° and ΔV° values is inadequate. The experimental data of Fe-Mg partitioning were taken at 22–47 GPa while an accurate

value of ΔV° is available only at ambient conditions. Thus, there is a large difference in pressure for these two types of data. In order to clarify this issue, further systematic studies, such as the examination of Fe-Mg partitioning over a wider range of composition, are needed.

4.2. Distinctive Effects of Pressure and Bulk Composition

[21] In order to discuss Fe-Mg partitioning between Pv and Mw in realistic lower mantle compositions, thermody-

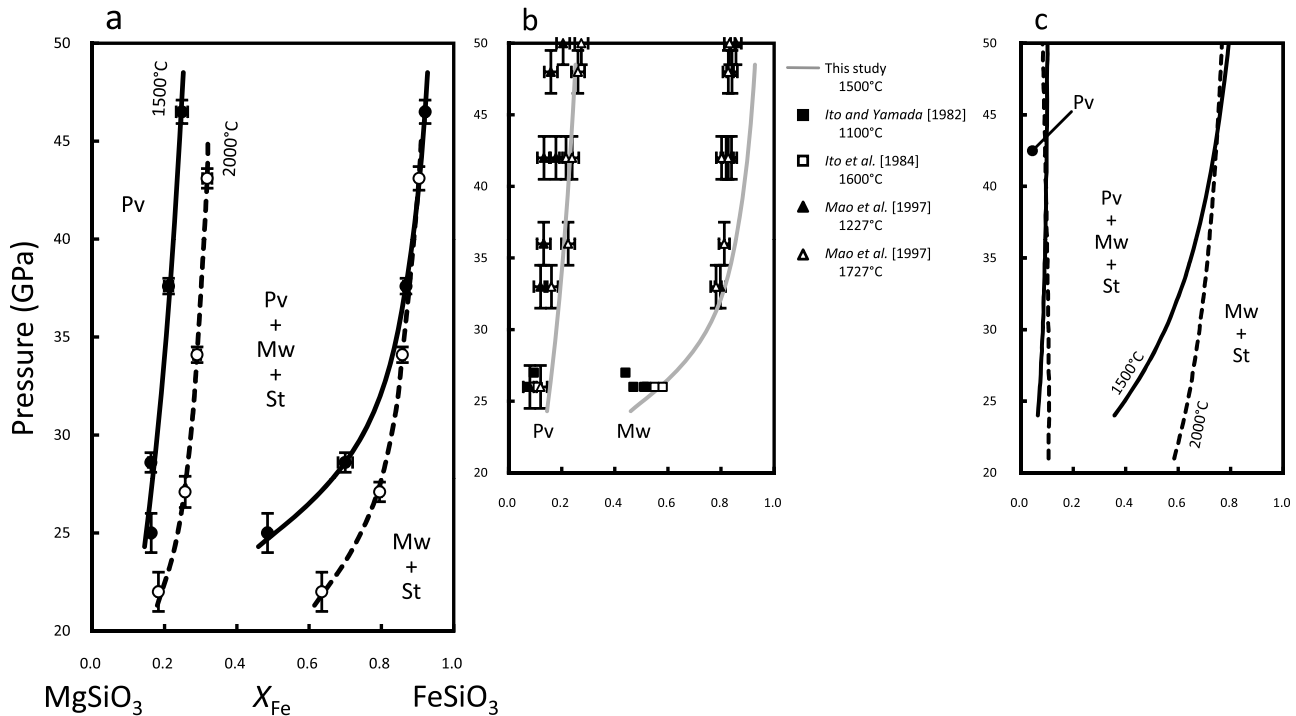


Figure 6. Pseudobinary phase diagrams in the system MgSiO₃-FeSiO₃. (a) Univariant compositions of Pv and Mw determined in this study and the corresponding phase boundaries. (b) Previously reported univariant compositions of Pv and Mw along with the present results. (c) Thermodynamically calculated phase boundaries using thermodynamic parameters reported by Akaoji *et al.* [1998].

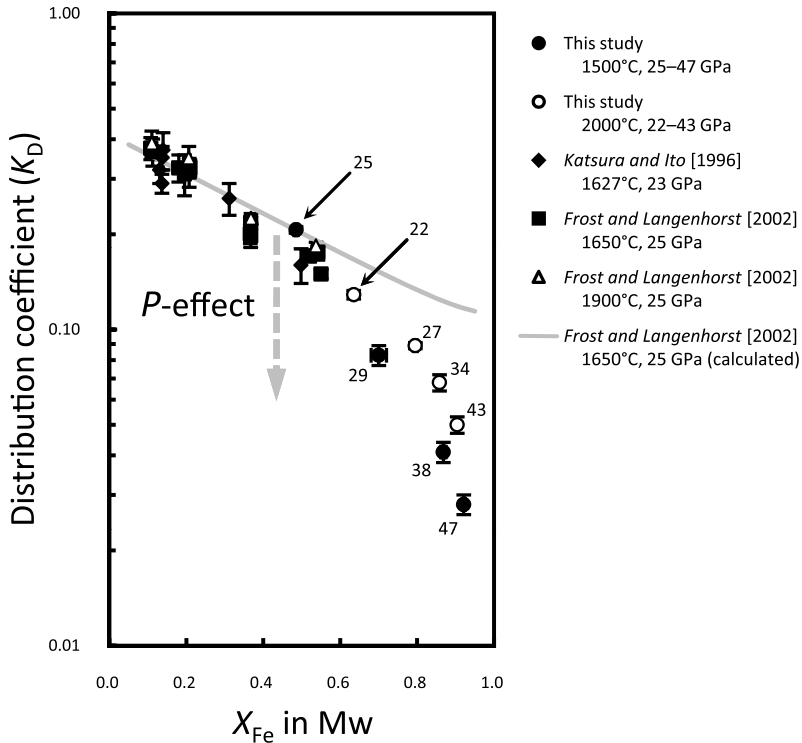


Figure 7. Fe-Mg distribution coefficients (K_D) between Pv and Mw as a function of iron content in Mw. The K_D values are calculated as $K_D = (X_{\text{Fe}}^{\text{Pv}}/X_{\text{Mg}}^{\text{Pv}})/(X_{\text{Fe}}^{\text{Mw}}/X_{\text{Mg}}^{\text{Mw}})$, and pressures in this study are shown around symbols. A gray line represents the calculated K_D based on W^{Pv} , W^{Mw} , and ΔG° determined by Frost and Langenhorst [2002].

namic calculations were carried out applying our experimental result to the magnesium-rich side of the studied system. The thermodynamic calculations were simply carried out on the basis of the symmetric regular solution model (equations (2) and (3)) with the fixed nonideal parameters for Pv and Mw: $W^{\text{Pv}} = 1650 \text{ J/mol}$ and $W^{\text{Mw}} = 12000 \text{ J/mol}$ [Frost and Langenhorst, 2002]. Applying our experimental results at 25–47 GPa and 1500°C to the thermodynamic model, Fe-Mg partitioning between Pv and Mw were calculated as functions of pressure and bulk composition at 1500°C. The considered bulk compositions are shown in the MgO-FeO-SiO₂ system at Figure 8a.

[22] At first, Fe-Mg partitioning between Pv and Mw were calculated in $(\text{Mg},\text{Fe})_2\text{SiO}_4$ olivine bulk compositions, varying the Fe/(Mg + Fe) ratio. The calculated K_D values at 1500°C for Fo₇₀, Fo₈₀, and Fo₉₀ are shown as a function of pressure, where Fo₇₀ denotes the composition of $(\text{Mg}_{0.7},\text{Fe}_{0.3})_2\text{SiO}_4$ (Figure 8b). The calculated K_D increases with decreasing Fe/(Mg + Fe) ratio (Fo₇₀ to Fo₉₀) at a constant pressure, and decreases with increasing pressure such as the experimental results at the most iron-rich ends (Figure 7).

[23] According to the pyrolite model [Ringwood, 1975], the bulk composition of the Earth's upper mantle has Fe/(Mg + Fe) ~0.1 and Si/(Mg + Fe) ~0.7, but the bulk composition of the lower mantle is highly uncertain and could be rather Si-rich [e.g., Ito *et al.*, 1984; Yagi and Funamori, 1996]. Thus we next calculated iron contents of coexisting Pv and Mw as a function of pressure varying the Si/(Mg + Fe) ratio of the bulk composition with the

Fe/(Mg + Fe) ratio fixed however at 0.1. In this case the proportion of Mw decreases with increasing bulk Si/(Mg + Fe) ratio. A remarkable Fe enrichment in Mw is expected at the highest pressures in Si-rich bulk compositions compared to olivine bulk compositions (Figure 8c). In the thermodynamic calculations at 2000°C, similar results were obtained as those at 1500°C described above.

4.3. Comparison With Previous Studies

[24] The calculated K_D values in Fo₉₀ at 25–47 GPa and 1500°C (Figure 8b) are compared with previous results performed by KMA or LHDAC in Al-free olivine bulk compositions, and the Fe-Mg distribution coefficients between Pv and Mw are summarized as a function of pressure in Figure 9. Detailed experimental conditions in each study are summarized in Table 4. Our calculated K_D shows good agreement with the previous results using KMA at ~25 GPa within errors [Katsura and Ito, 1996; Frost and Langenhorst, 2002] (Figure 9a). In addition, the smaller values of K_D above 40 GPa are consistent with the results with LHDAC determined by ATEM analyses of Kobayashi *et al.* [2005]. Auzende *et al.* [2008] performed the partitioning experiments in $(\text{Mg}_{0.9},\text{Fe}_{0.1})_2\text{SiO}_4$ olivine using LHDAC and analyzed recovered samples using ATEM and nano-SIMS. They reported higher K_D values than those of Kobayashi *et al.* [2005] at pressures below 80 GPa. The inconsistency in the K_D between the two LHDAC studies is possibly due to the differences in temperature conditions in the sample syntheses. Auzende *et al.* [2008] synthesized the sample at 400–950°C higher

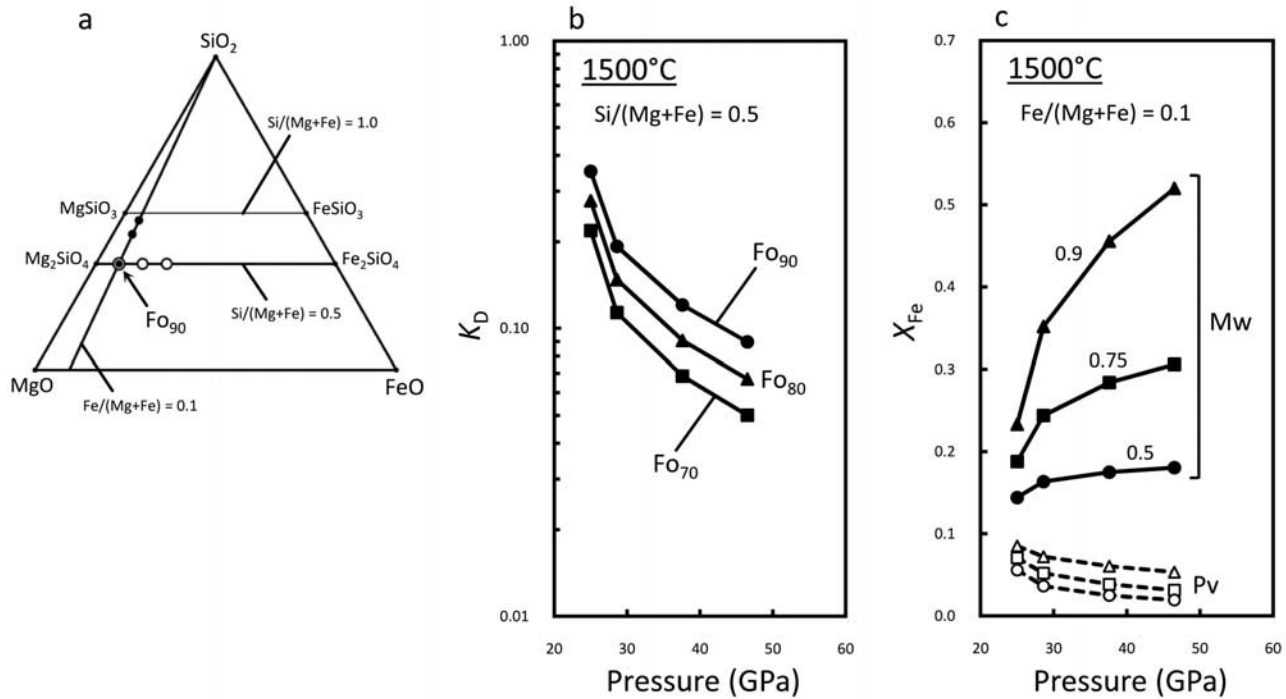


Figure 8. Fe-Mg partitioning between Pv and Mw at 1500°C in various bulk compositions (Figure 8a), and the calculated K_D (Figure 8b) and X_{Fe} of Pv and Mw (Figure 8c) as a function of pressure. (a) Calculated bulk compositions in the MgO-FeO-SiO₂ ternary diagram. Open symbols, olivine bulk compositions calculated in Figure 8b; solid symbols, compositions with $Fe/(Mg + Fe) = 0.1$ calculated in Figure 8c. Fo₉₀ is calculated in the both case. (b) K_D values in three olivine bulk compositions as a function pressure. The bulk $Fe/(Mg + Fe)$ is varied from 0.1 to 0.3. (c) X_{Fe} of coexisting Pv (open symbols and dashed lines) and Mw (solid symbols and lines) in three different bulk compositions as a function of pressure. The bulk $Si/(Mg + Fe)$ ratio is varied as 0.5, 0.75, and 0.9. Errors in the calculation correspond to symbol sizes, and circle symbols indicate Fo₉₀ in both diagrams.

condition than Kobayashi *et al.* [2005] did (Table 4). Before this study there was a large discrepancy between the results determined using KMA at ~ 25 GPa ($K_D > 0.3$) and results determined using laser-heated diamond anvil (LHDA) at the higher pressures ($K_D \sim 0.1$). This study has clarified that this is due to significant pressure dependence in Fe-Mg partitioning between Pv and Mw at pressures between 25 and 40 GPa. Mao *et al.* [1997] and Andrault [2001] reported K_D values based on XRD measurements (without chemical analyses). Although the reported K_D values are consistent with our calculated K_D around 30 GPa, they showed an opposite pressure dependence at the higher pressures than 40 GPa (Figure 9b). This inconsistency is probably due to large uncertainties in the chemical compositions of Pv and Mw determined by XRD.

[25] In Al-bearing bulk compositions, it is known that iron couples with aluminum in its ferric state and apparent K_D values become larger than those in Al-free systems, when we calculate K_D using total iron contents ($Fe_{total} = Fe^{2+} + Fe^{3+}$) [e.g., Wood and Rubie, 1996; Frost and Langenhorst, 2002]. Nishiyama and Yagi [2003] performed high $P-T$ experiments on a pyrolyte bulk composition at 30 GPa using KMA with SD anvils. They reported a higher K_D value than those of corresponding results

performed in the Al-free olivine composition with KMA at 25 GPa, where chemical compositions were measured by EPMA. Likewise, Murakami *et al.* [2005] reported higher K_D values than those reported for Al-free compositions in a similar peridotitic bulk composition (KLB-1) above 38 GPa using LHDA with ATEM analyses. Interestingly, in the Al-bearing peridotitic bulk compositions there is a gap in K_D values between 30 GPa and 38 GPa, and K_D values drop from 1.3 to 0.4 (Figure 9a). The Al³⁺ contents in Pv are to be constant in $P-T$ conditions where the garnet phase completely disappears (> 30 GPa) in the fixed bulk compositions. Additionally, the Fe³⁺ contents in Pv might be constant because the Fe³⁺ contents strongly relate (almost couple) to the Al³⁺ contents [Frost and Langenhorst, 2002]. Therefore the pressure effects on Fe²⁺-Mg partitioning determined in this study possibly affect the Fe_{total}-Mg partitioning in Al-bearing systems. It is considered that the inconsistency in the K_D values between those of Nishiyama and Yagi [2003] and Murakami *et al.* [2005] represent the pressure effect.

5. Conclusions

[26] We have summarized Fe-Mg partitioning between Pv and Mw in terms of pressure, and have shown the de-creas-

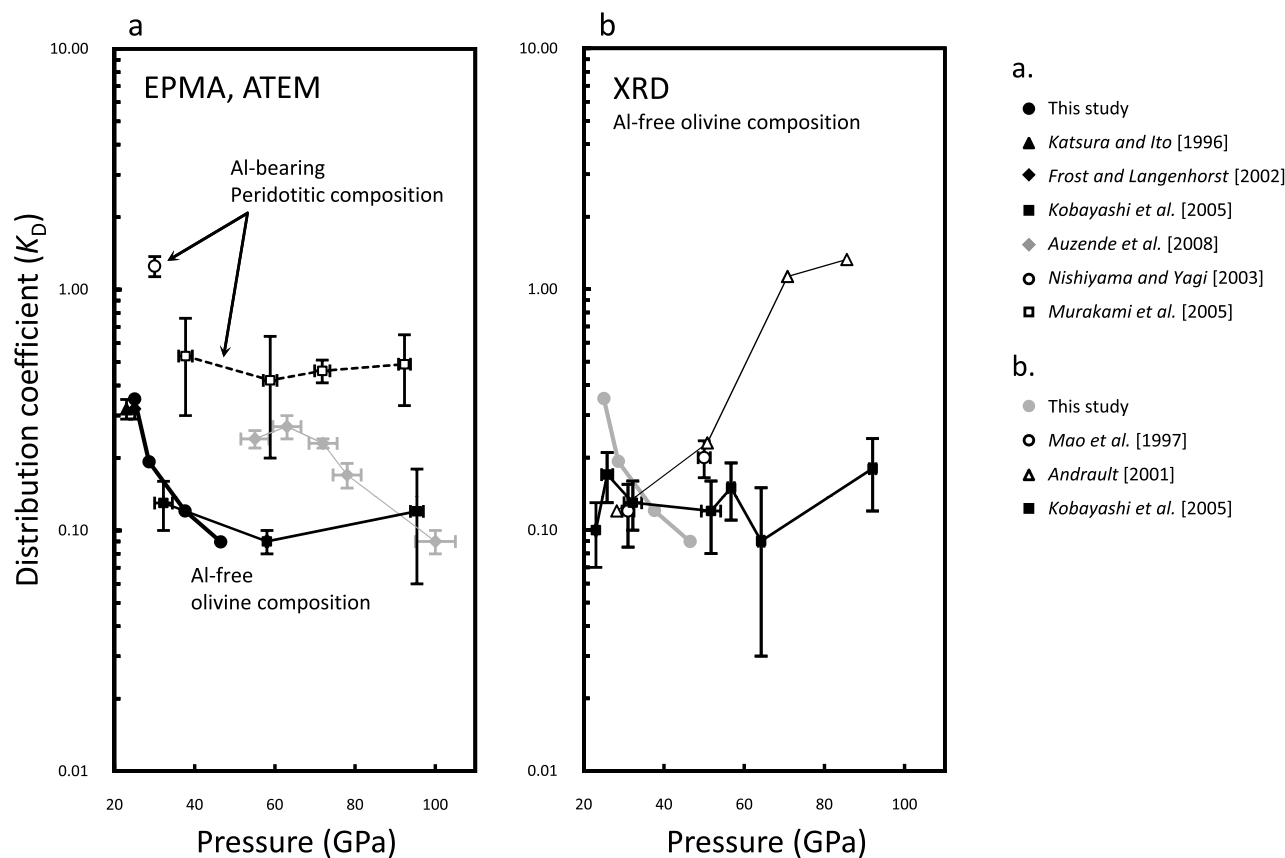


Figure 9. Comparison between thermodynamically calculated K_D values in Fo_{90} at 1500°C and previously reported values as a function of pressure. Detailed P - T - X conditions of each study are summarized in Table 4. (a) The K_D values based on chemical analyses using EPMA or ATEM. (b) Previously reported K_D values determined by XRD measurements along with the present results.

ing K_D in both experimental results and thermodynamic calculations in Al-free and Al-bearing bulk compositions (Figure 9a). This pressure dependence of Fe-Mg partitioning suggests the possibility of iron enrichment in Mw, and a compositional variation in Mw in lower mantle depths (Figure 8c). This might explain the observation that (Mg,Fe)O inclusions found in diamonds have iron contents ranging from 10 to 30 mol % [Harte et al., 1999]. In addition, the presence of highly iron-rich magnesiowüstite would have some influences on deep mantle properties such

as electric conductivity [e.g., Dobson et al., 1997] and viscosity [e.g., Long et al., 2006].

[27] It is clear that more studies are needed for a complete understanding of the phase relations in the system MgO-FeO-SiO₂ at P - T conditions of the Earth's lower mantle. The spin state transition of iron in Mw and Pv, and its influence on the Fe-Mg partitioning between Pv and Mw have been argued [e.g., Badro et al., 2003]. It is reported that the spin transition from a high-spin state to a mixed spin state starts from relatively low pressures (~35 GPa) in Mw with

Table 4. Distribution Coefficients Between Perovskite and Magnesiowüstite

Composition	Pressure (GPa)	Temperature (°C)	K_D^a	Synthesis	Analysis	Reference
<i>Al-Free Olivine Composition</i>						
Fo ₉₀ (calculated)	25–47	1500	0.09–0.35	KMA	EPMA, ATEM	this study
Fo ₉₁	23	1627	0.32	KMA	EPMA	Katsura and Ito [1996]
Fo ₈₈ (Opx + Mw)	25	1650	0.32	KMA	EPMA	Frost and Langenhorst [2002]
Fo ₈₂	31–50	1227	0.12–0.20	LHDAC	XRD	Mao et al. [1997]
Fo ₈₄	28–86	~1927	0.12–1.33	LHDAC	XRD	Andrault [2001]
Fo ₈₈ (Fo ₈₈ –Fo ₉₄) ^b	23–95	1227, 1327	0.09–0.18	LHDAC	ATEM, XRD	Kobayashi et al. [2005]
Fo ₉₀ (Fo ₉₃ –Fo ₉₅) ^b	55–100	1730–2180	0.09–0.27	LHDAC	ATEM, nano-SIMS	Auzende et al. [2008]
<i>Al-Bearing Peridotitic Composition</i>						
Pyrolite	30	1600	1.31	KMA	EPMA	Nishiyama and Yagi [2003]
KLB-1	38–92	1727–2027	0.4–0.5	LHDAC	ATEM	Murakami et al. [2005]

$$^a K_D = (X_{\text{Fe}}^{\text{Pv}}/X_{\text{Mg}}^{\text{Pv}})/(X_{\text{Fe}}^{\text{Mw}}/X_{\text{Mg}}^{\text{Mw}}).$$

^bTotal iron contents in the mineral assemblage of Pv and Mw were less than the starting compositions, and the compositions in parentheses represent the bulk mineral composition after syntheses.

compositions of $X_{\text{Fe}} \sim 0.17$ [Lin *et al.*, 2005; Tsuchiya *et al.*, 2006]. The spin transition of iron in Pv and Mw may have a significant influence on the phase relations in the MgO-FeO-SiO₂ system as well as on the physical and chemical properties of relevant minerals. The effect of the spin transition is not discussed in this study because not much is known on the thermodynamic and thermoelastic properties of Pv and Mw with low-spin states. However, the discrepancy of the ΔV° value inferred from Mg-Fe partitioning and that determined by volume measurements at ambient conditions may be partly due to the spin transition. As demonstrated in this study, the experimental technique using KMA with SD anvils is a powerful tool to investigate phase equilibria at P - T conditions of the Earth's lower mantle. Therefore, it is expected that further systematic studies using KMA with SD anvils will improve our understanding of lower mantle mineralogy.

[28] **Acknowledgments.** We thank Y. Nakajima, S. Ono, and A. Nozawa for their assistance during synchrotron experiments; M. Murakami and K. Hirose for help and advice with ATEM analyses; and T. Suzuki, K. Kawamura, and J. Tuff for comments on an earlier version of this manuscript. We are grateful to Y. Fei, D. J. Frost, and D. Andrault for the constructive reviews and comments. This study is based on research proposals to SPring-8 (2003B0411, 2004B0437-ND2b-np, 2004A3892-PU1-np) with a Grant-in-Aid for Scientific Research from the Japanese government (to E. Takahashi; 12002006, 18204050) and Research Fellowships for Young Scientists from the Japan Society for the Promotion of Science (to Y. Tange; 03356).

References

- Akaogi, M., H. Kojitani, K. Matsuzaka, T. Suzuki, and E. Ito (1998), Postspinel transformations in the system Mg₂SiO₄-Fe₂SiO₄: Element partitioning, calorimetry, and thermodynamic calculation, in *Properties of Earth and Planetary Materials at High Pressure and Temperature, Geophys. Monogr. Ser.*, vol. 101, edited by M. H. Manghnani and T. Yagi, pp. 373–384, AGU, Washington, D. C.
- Andrault, D. (2001), Evaluation of (Mg,Fe) partitioning between silicate perovskite and magnesiowüstite up to 120 GPa and 2300 K, *J. Geophys. Res.*, **106**, 2079–2087, doi:10.1029/2000JB900362.
- Andrault, D., G. Fiquet, F. Guyot, and M. Hanfland (1998), Pressure induced Landau-type transition in stishovite, *Science*, **282**, 720–724, doi:10.1126/science.282.5389.720.
- Andrault, D., R. J. Angel, J. L. Mosenfelder, and T. Le Bihan (2003), Equation of state of stishovite to lower mantle pressures, *Am. Mineral.*, **88**, 301–307.
- Auzende, A.-L., J. Badro, F. J. Ryerson, P. K. Weber, S. J. Fallon, A. Addad, J. Siebert, and G. Fiquet (2008), Element partitioning between magnesium silicate perovskite and ferropericlase: New insights into bulk lower-mantle geochemistry, *Earth Planet. Sci. Lett.*, **269**, 164–174, doi:10.1016/j.epsl.2008.02.001.
- Badro, J., G. Fiquet, F. Guyot, J. S. Rueff, V. V. Struzhkin, G. Vanko, and G. Monaco (2003), Iron partitioning in Earth's mantle: Toward a deep lower mantle discontinuity, *Science*, **300**, 789–791, doi:10.1126/science.1081311.
- Dobson, D. P., N. C. Richmond, and J. P. Brodholt (1997), A high-temperature electrical conduction mechanism in the lower mantle phase (Mg,Fe)_{1-x}O, *Science*, **275**, 1779–1781, doi:10.1126/science.275.5307.1779.
- Endo, S., T. Akai, Y. Akahama, M. Wakatsuki, T. Nakamura, Y. Tomii, K. Koto, Y. Ito, and M. Tokonami (1986), High temperature X-ray study of single crystal stishovite synthesized with Li₂WO₄ as flux, *Phys. Chem. Miner.*, **13**, 146–151, doi:10.1007/BF00308155.
- Fei, Y., Y. Wang, and L. W. Finger (1996), Maximum solubility of FeO in (Mg,Fe)SiO₃-perovskite as a function of temperature at 26 GPa: Implication for FeO content in the lower mantle, *J. Geophys. Res.*, **101**, 11,525–11,530, doi:10.1029/96JB00408.
- Fiquet, G., D. Andrault, A. Dewaele, T. Charpin, M. Kunz, and D. Husermann (1998), P - V - T equation of state of MgSiO₃ perovskite, *Phys. Earth Planet. Inter.*, **105**, 21–31, doi:10.1016/S0031-9201(97)00077-0.
- Frost, D. J., and F. Langenhorst (2002), The effect of Al₂O₃ on Fe-Mg partitioning between magnesiowüstite and magnesium silicate perovskite, *Earth Planet. Sci. Lett.*, **199**, 227–241, doi:10.1016/S0012-821X(02)00558-7.
- Funamori, N., T. Yagi, W. Utsumi, T. Kondo, T. Uchida, and M. Funamori (1996), Thermoelastic properties of MgSiO₃ perovskite determined by in situ X-ray observations up to 30 GPa and 2000 K, *J. Geophys. Res.*, **101**, 8257–8269, doi:10.1029/95JB03732.
- Harte, B., J. W. Harris, M. T. Hutchison, G. R. Watt, and M. C. Wilding (1999), Lower mantle mineral associations in diamonds from São Luiz, Brazil, in *Mantle Petrology: Field Observations and High Pressure Experimentation*, edited by Y. Fei, C. Bertka, and B. O. Mysen, *Geochem. Soc. Spec. Publ.*, **6**, 125–153.
- Ito, E., and Y. Matsui (1978), Synthesis and crystal-chemical characterization of MgSiO₃ perovskite, *Earth Planet. Sci. Lett.*, **38**, 443–450, doi:10.1016/0012-821X(78)90119-X.
- Ito, E., and E. Takahashi (1989), Postspinel transformations in the system Mg₂SiO₄-Fe₂SiO₄ and some geophysical implications, *J. Geophys. Res.*, **94**, 10,637–10,646, doi:10.1029/JB094iB08p10637.
- Ito, E., and H. Yamada (1982), Stability relations of silicate spinels, ilmenites, and perovskites, in *High-Pressure Research in Geophysics*, edited by S. Akimoto and M. H. Manghnani, pp. 405–419, Cent. Acad. Publ. Jpn, Tokyo.
- Ito, E., E. Takahashi, and Y. Matsui (1984), The mineralogy and chemistry of the lower mantle: An implication of the ultrahigh-pressure phase relations in the system MgO-FeO-SiO₂, *Earth Planet. Sci. Lett.*, **67**, 238–248, doi:10.1016/0012-821X(84)90119-5.
- Ito, E., T. Katsura, Y. Aizawa, K. Kawabe, S. Yokoshi, A. Kubo, A. Nozawa, and K. Funakoshi (2005), High-pressure generation in the Kawai-type apparatus equipped with sintered diamond anvils: Application to the wurtzite-rocksalt transformation in GaN, in *Advances in High-Pressure Technology for Geophysical Applications*, edited by J. Chen et al., pp. 451–460, Elsevier, Amsterdam.
- Ito, H., K. Kawada, and S. Akimoto (1974), Thermal expansion of stishovite, *Phys. Earth Planet. Inter.*, **8**, 277–281, doi:10.1016/0031-9201(74)90094-6.
- Katsura, T., and E. Ito (1996), Determination of Fe-Mg partitioning between perovskite and magnesiowüstite, *Geophys. Res. Lett.*, **23**, 2005–2008, doi:10.1029/96GL02086.
- Katsura, T., K. Funakoshi, A. Kubo, N. Nishiyama, Y. Tange, Y. Sueda, T. Kubo, and W. Utsumi (2004), A large-volume high-pressure and high-temperature apparatus for in situ X-ray observation, ‘SPEED-Mk.II’, *Phys. Earth Planet. Inter.*, **143–144**, 497–506, doi:10.1016/j.pepi.2003.07.025.
- Kawai, N., and S. Endo (1970), The generation of ultrahigh hydrostatic pressure by a split sphere apparatus, *Rev. Sci. Instrum.*, **4**, 425–428.
- Kobayashi, Y., T. Kondo, E. Ohtani, N. Hirao, N. Miyajima, T. Yagi, T. Nagase, and T. Kikegawa (2005), Fe-Mg partitioning between (Mg,Fe)SiO₃ post-perovskite, perovskite, and magnesiowüstite in the Earth's lower mantle, *Geophys. Res. Lett.*, **32**, L19301, doi:10.1029/2005GL023257.
- Lin, J. F., V. V. Struzhkin, S. D. Jacobsen, M. Y. Hu, P. Chow, J. Kung, H. Lin, H. K. Mao, and R. J. Hemley (2005), Spin transition of iron in magnesiowüstite in the Earth's lower mantle, *Nature*, **436**, 377–380, doi:10.1038/nature03825.
- Liu, J., J. Zhang, L. Flesch, B. Li, D. J. Weidner, and R. C. Liebermann (1999), Thermal equation of state of stishovite, *Phys. Earth Planet. Inter.*, **112**, 257–266, doi:10.1016/S0031-9201(99)00037-0.
- Liu, L. G. (1974), Silicate perovskite from phase transformations of pyrope-garnet at high pressure and temperature, *Geophys. Res. Lett.*, **4**, 299–305.
- Long, M. D., X. Xiao, Z. Jiang, B. Evans, and S. Karato (2006), Lattice preferred orientation in deformed polycrystalline (Mg,Fe)O and implications for seismic anisotropy in D, *Phys. Earth Planet. Inter.*, **156**, 75–88, doi:10.1016/j.pepi.2006.02.006.
- Mao, H. K., R. J. Hemley, Y. Fei, J. F. Shu, L. C. Chen, A. P. Jephcoat, Y. Wu, and W. A. Bassett (1991), Effect of pressure, temperature, and composition on lattice parameters and density of (Fe,Mg)SiO₃-perovskites to 30 GPa, *J. Geophys. Res.*, **96**, 8069–8079, doi:10.1029/91JB00176.
- Mao, H.-K., G. Shen, and R. J. Hemley (1997), Multivariable dependence of Fe-Mg partitioning in the lower mantle, *Science*, **278**, 2098–2100, doi:10.1126/science.278.5346.2098.
- Murakami, M., K. Hirose, N. Sata, and Y. Ohishi (2005), Post-perovskite phase transition and mineral chemistry in the pyrolytic lowermost mantle, *Geophys. Res. Lett.*, **32**, L03304, doi:10.1029/2004GL021956.
- Nishihara, Y., K. Nakayama, E. Takahashi, T. Iguchi, and K. Funakoshi (2005), P - V - T equation of state of stishovite to the mantle transition zone conditions, *Phys. Chem. Miner.*, **31**, 660–670, doi:10.1007/s00269-004-0426-7.
- Nishiyama, N., and T. Yagi (2003), Phase relation and mineral chemistry in pyrolyte to 2200°C under the lower mantle pressures and implications for dynamics of mantle plumes, *J. Geophys. Res.*, **108(B5)**, 2255, doi:10.1029/2002JB002216.

- Ono, S., T. Katsura, and E. Ito (2001), In situ observation of ilmenite-perovskite phase transition in MgSiO₃ using synchrotron radiation, *Geophys. Res. Lett.*, 28, 835–838, doi:10.1029/1999GL008446.
- Ringwood, A. E. (1975), *Composition and Petrology of the Earth's Mantle*, 618 pp., McGraw-Hill, New York.
- Ross, N. L., J.-F. Shu, and R. M. Hazen (1990), High-pressure crystal chemistry of stishovite, *Am. Mineral.*, 75, 739–747.
- Takafuji, N., K. Hirose, S. Ono, F. Xu, M. Mitome, and Y. Bando (2004), Segregation of core melts by permeable flow in the lower mantle, *Earth Planet. Sci. Lett.*, 224, 249–257, doi:10.1016/j.epsl.2004.05.016.
- Tange, Y., T. Irfune, and K. Funakoshi (2008), Pressure generation to 80 GPa using multianvil apparatus with sintered diamond anvils, *High Pressure Res.*, 28, 245–254, doi:10.1080/08957950802208936.
- Tsuchiya, T. (2003), First-principles prediction of the *P-V-T* equation of state of gold and the 660-km discontinuity in Earth's mantle, *J. Geophys. Res.*, 108(B10), 2462, doi:10.1029/2003JB002446.
- Tsuchiya, T., R. M. Wentzcovitch, C. R. S. da Silva, and S. de Gironcoli (2006), Spin transition in magnesiowüstite in Earth's lower mantle, *Phys. Rev. Lett.*, 96, 198501, doi:10.1103/PhysRevLett.96.198501.
- Tuff, J., E. Takahashi, and S. A. Gibson (2005), Experimental constraints on the role of garnet pyroxenite in the genesis of high-Fe mantle plume derived melts, *J. Petrol.*, 46, 2023–2058, doi:10.1093/petrology/egi046.
- Utsumi, W., K. Funakoshi, S. Urakawa, M. Yamakata, K. Tsuji, H. Konishi, and O. Shimomura (1998), SPring-8 beamlines for high pressure science with multi-anvil apparatus, *Rev. High Press. Sci. Technol.*, 7, 1484–1486.
- Wang, Y., D. J. Weidner, R. C. Liebermann, and Y. Zhao (1994), *P-V-T* equation of state of (Mg,Fe)SiO₃ perovskite: Constraints on composition of the lower mantle, *Phys. Earth Planet. Inter.*, 83, 13–40, doi:10.1016/0031-9201(94)90109-0.
- Watanuki, T., O. Shimomura, T. Yagi, T. Kondo, and M. Isshiki (2001), Construction of laser-heated diamond anvil cell system for in situ X-ray diffraction study at SPring-8, *Rev. Sci. Instrum.*, 72, 1289–1292, doi:10.1063/1.1343869.
- Wood, B. J., and D. C. Rubie (1996), The effect of alumina on phase transformations at the 660-kilometer discontinuity from Fe-Mg partitioning experiments, *Science*, 273, 1522–1524, doi:10.1126/science.273.5281.1522.
- Yagi, T., and N. Funamori (1996), Chemical composition of the lower mantle inferred from the equation of state of MgSiO₃ perovskite, *Philos. Trans. R. Soc. London*, 354, 1371–1384, doi:10.1098/rsta.1996.0053.
- Yagi, T., H. K. Mao, and P. M. Bell (1978), Structure and crystal chemistry of perovskite-type MgSiO₃, *Phys. Chem. Miner.*, 3, 97–110, doi:10.1007/BF00308114.
- Yagi, T., P. M. Bell, and H. K. Mao (1979a), Phase Relations in the system MgO-FeO-SiO₂ between 150 and 700 kbar at 1000°C, *Carnegie Inst. Washington Year Book*, 78, 614–618.
- Yagi, T., P. M. Bell, and H. K. Mao (1979b), Lattice parameters and specific volume for perovskite phase of orthopyroxene composition (Mg,Fe)SiO₃, *Carnegie Inst. Washington Year Book*, 78, 612–613.
- Yamanaka, T., T. Fukuda, and J. Tsuchiya (2002), Bonding character of SiO₂ stishovite under high pressures up to 30 GPa, *Phys. Chem. Miner.*, 29, 633–641, doi:10.1007/s00269-002-0257-3.

K. Funakoshi, Japan Synchrotron Radiation Research Institute, 1-1-1 Kouto, Sayo-cho, Sayo-gun, Hyogo 679-5198, Japan. (funakosi@spring8.or.jp)

Y. Nishihara and Y. Tange, Geodynamics Research Center, Ehime University, 2-5 Bunkyo-cho, Matsuyama, Ehime 790-8577, Japan. (yunishi@sci.ehime-u.ac.jp; tan@sci.ehime-u.ac.jp)

N. Sata, Institute for Research on Earth Evolution, Japan Agency for Marine-Earth Science and Technology, 2-15 Natsushima, Yokosuka, Kanagawa 237-0061, Japan. (sata@jamstec.go.jp)

E. Takahashi, Department of Earth and Planetary Sciences, Tokyo Institute of Technology, 2-12-1 Ookayama, Meguro-ku, Tokyo 152-8551, Japan. (etakahas@geo.titech.ac.jp)